Electrodeposition of High-Surface-Area IrO$_2$ Films on Ti Felt as an Efficient Catalyst for the Oxygen Evolution Reaction

Yu Jin Park [1,2†], Jooyoung Lee [1†], Yoo Sei Park [1,2], Juchan Yang [1], Myeong Je Jang [1], Jaehoon Jeong [1], Seunghoe Choe [1], Jung Woo Lee [2*], Jung-Dae Kwon [1*] and Sung Mook Choi [1*]

[1] Surface Technology Division, Materials Center for Energy Department, Korea Institute of Materials Science, Changwon, South Korea, [2] Department of Materials Science and Engineering, Pusan National University, Busan, South Korea

Under acidic conditions, IrO$_2$ exhibits high catalytic activity with respect to the oxygen evolution reaction (OER). However, the practical application of Ir-based catalysts is significantly limited owing to their high cost in addition to the scarcity of the metal. Therefore, it is necessary to improve the efficiency of the utilization of such catalysts. In this study, IrO$_2$-coated Ti felt (IrO$_2$/Ti) electrodes were prepared as high-efficiency catalysts for the OER under acidic conditions. By controlling the surface roughness of the Ti substrate via wet etching, the optimum Ti substrate surface area for application in the IrO$_2$/Ti electrode was determined. Additionally, the IrO$_2$ film that was electrodeposited on the 30 min etched Ti felt had a large surface area and a uniform morphology. Furthermore, there were no micro-cracks and the electrode obtained (IrO$_2$/Ti-30) exhibited superior catalytic performance with respect to the OER, with a mass activity of 362.3 A g$_{Ir}^{-1}$ at a potential of 2.0 V (vs. RHE) despite the low Ir loading (0.2 mg cm^{-2}). Therefore, this proposed strategy for the development of IrO$_2$/Ti electrodes with substrate surface control via wet etching has potential for application in the improvement of the efficiency of catalyst utilization with respect to the OER.

Keywords: wet etching, iridium oxide, oxygen evolution reaction, electrodeposition, surface area

INTRODUCTION

Hydrogen, which is a pollution-free energy resource with the convenience of long-term storage in small and large quantities without significant loss, has a number of distinct advantages as an alternative to fossil fuels (Bensaid et al., 2012; Nam et al., 2019). As a promising hydrogen production strategy, water electrolysis has emerged as a sustainable and eco-friendly technology (Brillet et al., 2012; Park et al., 2019b). Despite these benefits, one key reason it has not been utilized in practical applications is the slow associated rate of the oxygen evolution reaction (OER) (Zhou et al., 2020). The OER involves four electron-proton coupled reactions, and requires the use of a relatively higher amount of energy (higher overpotential) compared to the hydrogen evolution reaction (HER), which is a typical two electron-transfer reaction (Suen et al., 2017; Jang et al., 2020). To overcome these limitations, studies have been conducted with the aim to develop electrocatalysts to ensure the efficiency of the OER (Choi et al., 2018). Ir or Ru based catalysts demonstrate excellent

catalytic properties with respect to the OER; however, because they are noble metals, they tend to be more expensive and scarce (Guo et al., 2019; Park et al., 2020a). Conversely, non-noble-metal based OER electrocatalysts are less costly and more abundant. However, under acidic pH conditions they are susceptible to corrosion and often show poor catalytic activity (Jiang et al., 2019; Park et al., 2020b). Given that the economy of hydrogen production via electrolysis is primarily based on catalytic activity rather than on the cost of the catalyst employed (Kanan and Nocera, 2008; Dinca et al., 2010), noble-metal catalysts, such as Ir- or Ru-based catalysts, which are very rare, account for a high proportion of OER electrocatalysts (Smith et al., 2014). Thus, studies to investigate the efficient use of small amounts of these catalysts are necessary.

To prepare electrodes, the catalyst coating methods currently in use include powder coating (Su et al., 2011; Al-Shroofy et al., 2017), sputtering (Sapountzi et al., 2011; Xiaokai et al., 2019), and electrodeposition (Yagi et al., 2005; Lee et al., 2016). Powder coating can be applied to large area electrodes; however, this is associated with low conductivity, and causes significant catalyst loss. Further, the sputtering method is associated with high conductivity and offers the possibility of controlling the surface morphology of the electrode with great ease. Yet, its application results in poor uniformity when applied over a large surface area. This method can also result in the damage of the substrate owing to ion collision. In contrast, with the electrodeposition method, it is possible to coat a substrate with a uniform composition metal film to obtain a smooth surface (Maliar et al., 2019; Park et al., 2019a). Additionally, the electrodeposition method also enables low-cost deposition via direct growth, and it is associated with efficient catalyst utilization (Kim et al., 2004; Fouda-Onana et al., 2014). Therefore, this is used to prepare electrodes for electrochemical applications (Fan et al., 2018; Wang et al., 2018).

Substrate adhesion and surface area are important factors that influence the quality of the catalyst layer when electrodes are prepared using the electrodeposition (Chalker et al., 1991; Marzouk, 2003). Generally, the formation of the native oxide layer on the substrate owing to exposure to air increases contact resistance and decreases substrate adhesion, which can be enhanced by removing the native oxide layer (Bryce et al., 2010). To provide a corrosion-resistant protective film that inhibits substrate passivation and acts as a cost effective catalyst layer for the OER, Choe et al. (2018) proposed the use of electrodeposited IrO_2. However, studies on substrate surfaces for the electrodeposited IrO_2 catalyst are limited. Hence, further studies are required to ensure the efficient control of the substrate surface before the electrodeposition.

In this study, IrO_2/Ti electrodes were prepared via the electrodeposition of an iridium catalyst layer on a strong Ti felt in an acidic condition. To control the Ti felt surface and establish the optimal surface area, wet etching was employed, and the performances of the prepared electrodes with respect to the OER in acidic condition were investigated.

MATERIALS AND METHODS

Preparation of IrO_2/Ti Electrodes Using Anodic Electrodeposition

To prepare the electrodeposition solution, 0.1 M iridium chloride ($IrCl_4 \cdot H_2O$) was dissolved in DI water and stirred for 30 min. Then, 40 mM oxalic acid [$(COOH)_2 \cdot 2H_2O$] and 100 mM hydrogen peroxide (H_2O_2) were added, and the mixture was homogenized for 10 min. To adjust the pH to 10.5, 340 mM potassium carbonate (34.5% K_2CO_3) was added, followed by stirring for 3 days to ensure the stability of the prepared electrodeposition solution (Lee et al., 2015).

IrO_2/Ti electrodes were then prepared via electrodeposition on a titanium mesh (Ti gauze 80 mesh, Alpha Aeaser), which served as the substrate. Prior to the electrodeposition, etching with 5 wt.% oxalic acid was performed to remove any oxide layer or impurities that could be present on the Ti felt. Then, to observe the changes on the surface of the IrO_2/Ti electrode with respect to the etching time, etching was performed for 0, 10, 20, 30, and 40 min in the etchant at 95°C.

A three-electrode system was used for the anodic electrodeposition. The titanium mesh and the standard calomel electrode (SCE) were used as a counter and reference electrode, respectively, and IrO_2 electrodeposition was performed using a potentiostat (VMP-3, Bio-Logic, France) via the application of a constant current density of 2.5 mA cm^{-2} to the Ti felt for 10 min in the IrO_2 electrodeposition solution at 25°C. The reaction that took place in this anodic electrodeposition is as follows.

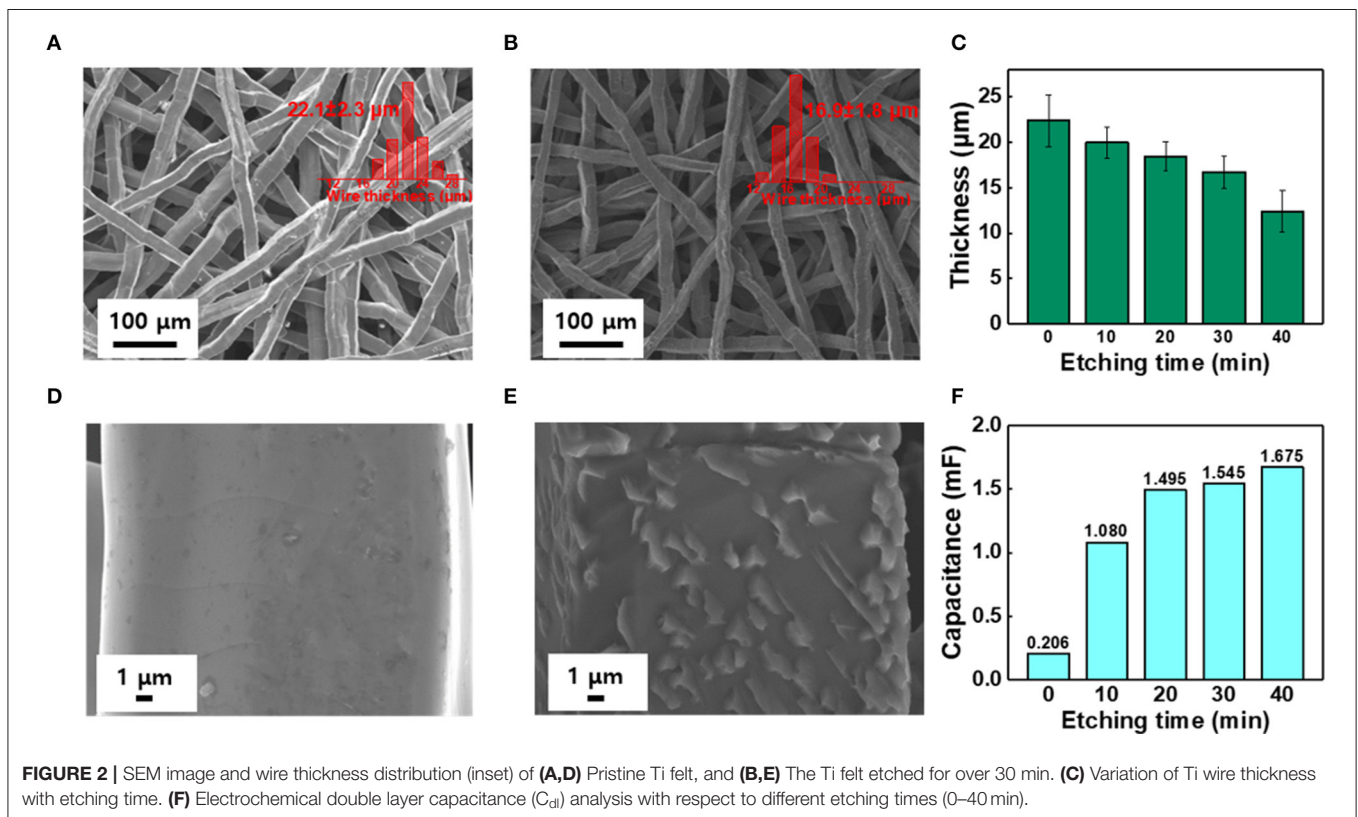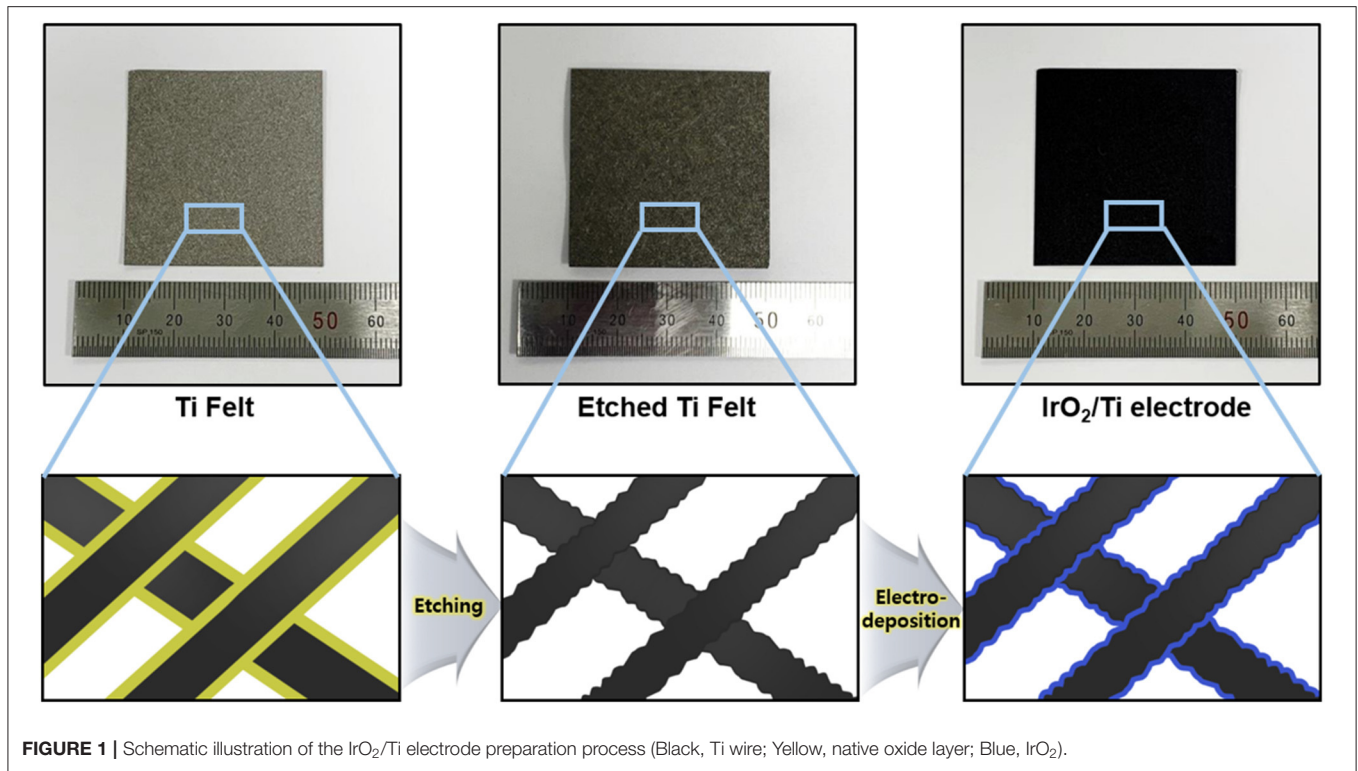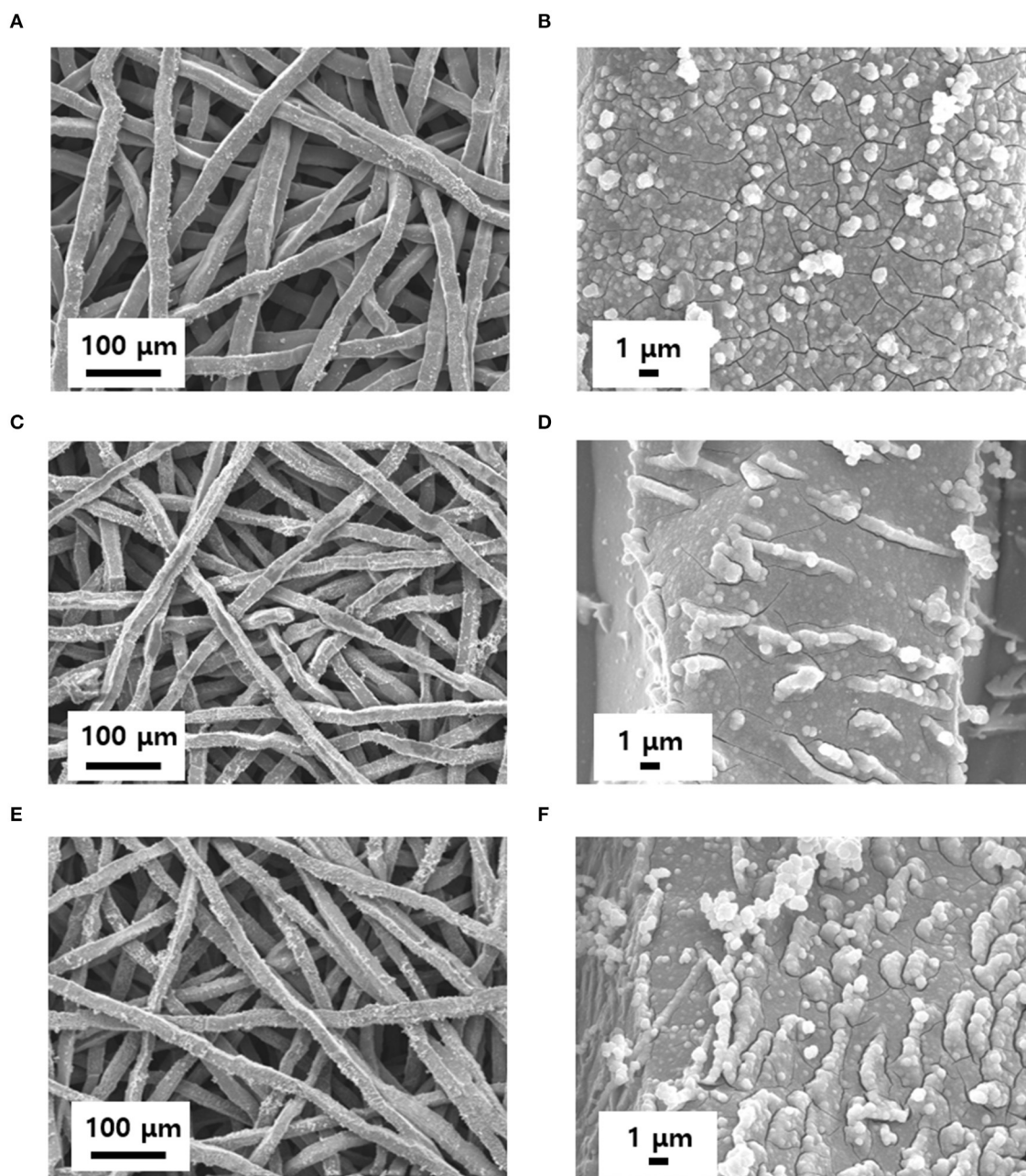$$[Ir(COO)_2(OH)_4]^{2-} \rightarrow IrO_2 + 2CO_2 + 2H_2O + 2e^-$$

Physicochemical Characterization

Field emission scanning electron microscopy (FE-SEM, JEOL, JSM-7001F) and optical microscopy (OM, MXG-2500REZ) were performed to observe the surface morphology of the prepared IrO_2/Ti electrodes. X-ray diffractometry (XRD, D/MAX 2500, Rigaku) was performed to observe the crystallinity of the IrO_2 layer. For the conditions for the XRD, a Cu target at 40 kV and 200 mA, with a 2θ angle in the range 30–80° and a scanning rate of 1° min^{-1}, was used. Additionally, the crystal structure of the IrO_2 film was analyzed via X-ray photoelectron spectroscopy (XPS, ECSA2000 VG Microtech) using an Al Kα (1486.6 eV) light source, and each peak was fitted with carbon (284.6 eV). Inductively coupled plasma-mass spectroscopy (ICP-MS, iCAP 6300 sermodero Ltd.) was employed to determine the loading mass of Ir.

Electrochemical Characterization

For the electrochemical characterization of the IrO_2/Ti electrode, linear sweep voltammetry (LSV) and stability tests were performed using a potentiostat (VMP-3, Bio-Logic, France). IrO_2/Ti (1 cm x 1 cm), Ag/AgCl (saturated KCl), and Pt were used as the working, reference, and counter electrodes of the three-electrode system, respectively. A 0.1 M solution of $HClO_4$ was used as the electrolyte, and the LSV was performed within a voltage range of 0.25–2.0 V (vs. RHE). Additionally, the stability tests were conducted via the application of a constant current

FIGURE 1 | Schematic illustration of the IrO$_2$/Ti electrode preparation process (Black, Ti wire; Yellow, native oxide layer; Blue, IrO$_2$).

FIGURE 2 | SEM image and wire thickness distribution (inset) of **(A,D)** Pristine Ti felt, and **(B,E)** The Ti felt etched for over 30 min. **(C)** Variation of Ti wire thickness with etching time. **(F)** Electrochemical double layer capacitance (C$_{dl}$) analysis with respect to different etching times (0–40 min).
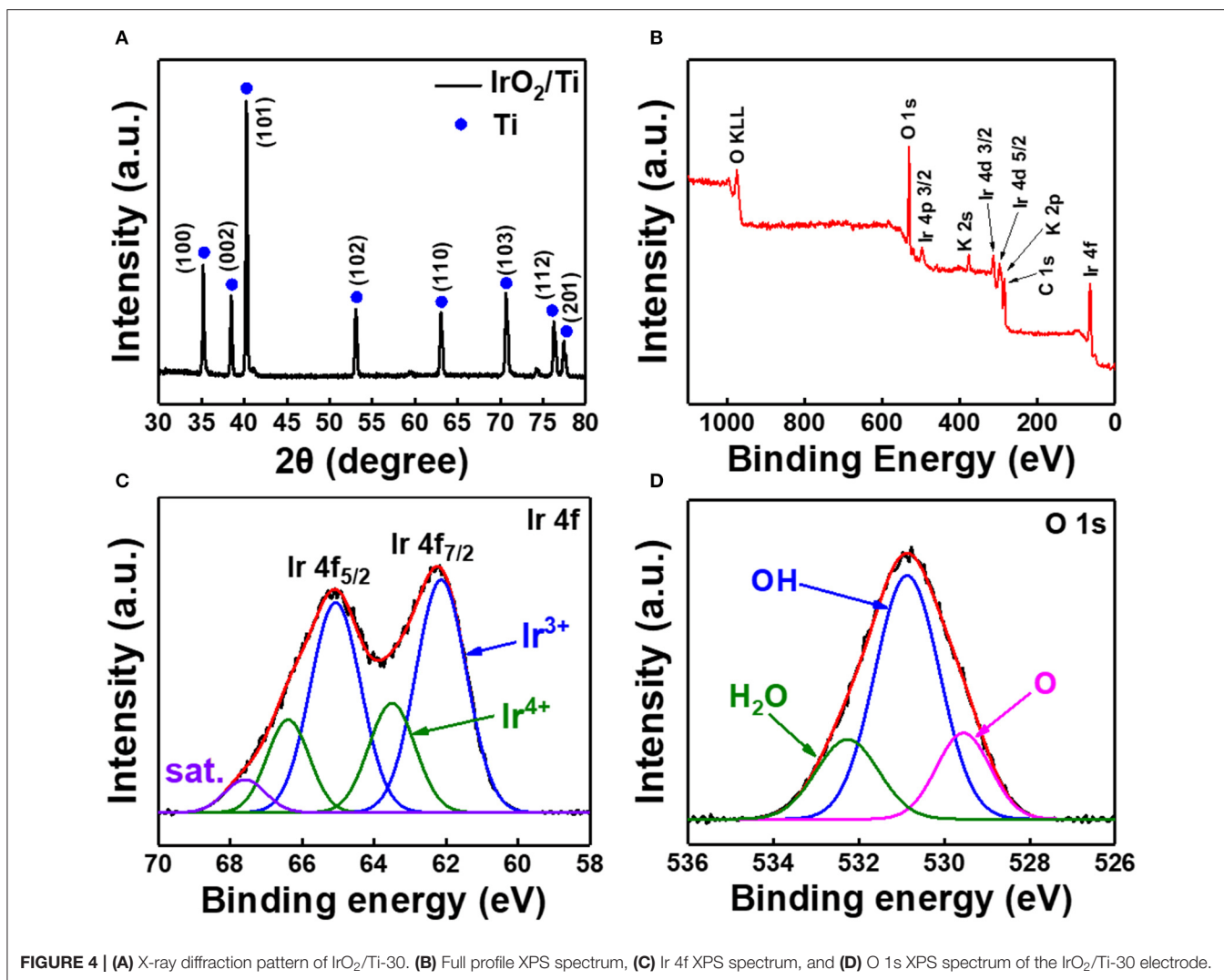
FIGURE 3 | Evolution of IrO_2/Ti morphology with time. The electrodes were prepared by controlling the etching time to: **(A,B)** 0, **(C,D)** 30, and **(E,F)** 40 min.

of 10 mA cm^{-2} for ∼800 min, and electrochemical impedance spectroscopy (EIS) was performed within a frequency range of 100–200 kHz at a potential of 1.34 V.

RESULTS AND DISCUSSION

To remove the oxide layer on the surface of the Ti felt and control its roughness, the Ti felt substrate was etched in 5 wt.% oxalic acid, which served as the etchant. The etching time was varied at 0, 10, 20, 30, and 40 min, and the electrodes
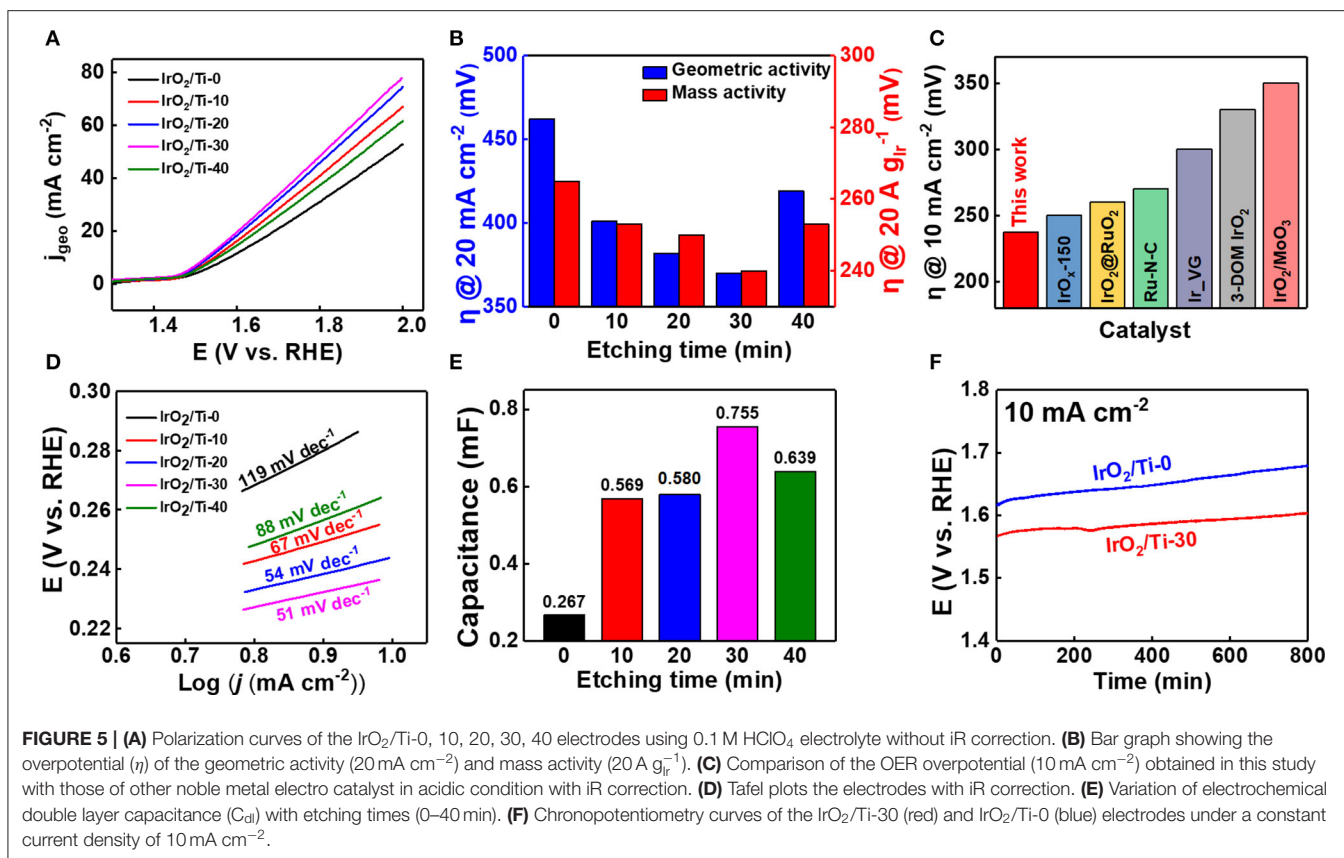
obtained were labeled IrO_2/Ti- 0, 10, 20, 30, and 40, respectively. After etching, a layer of IrO_2 was deposited on the Ti felt *via* the application of a current density of 2.5 mA cm^{-2} for 10 min at 25°C in an electrodeposition solution. Following the electrodeposition, the Ti felt was uniformly coated with the IrO_2 film (**Figure 1**). The variation of the surface morphology of the Ti felt as a function of the etching time, which was observed using a field emission scanning electron microscope (FE-SEM), is shown in **Figures 2A,B,D,E**. The wire thickness of the Ti felt decreased from 22.1 ± 2.3 μm (etching time:

FIGURE 4 | **(A)** X-ray diffraction pattern of IrO_2/Ti-30. **(B)** Full profile XPS spectrum, **(C)** Ir 4f XPS spectrum, and **(D)** O 1s XPS spectrum of the IrO_2/Ti-30 electrode.

0 min) to $16.9 \pm 1.8\,\mu m$ (etching time: 30 min), and after etching for 40 min, it had decreased significantly ($13.5 \pm 1.7\,\mu m$), and became brittle (**Figure 2C**). Generally, the thickness of the native oxide layer of Ti is 3–7 nm (**Supplementary Figure 1**) (Wang et al., 2016). Given that the thickness of the Ti felt was reduced by more than $\sim 2\,\mu m$ as a result of etching, it was reasonable to consider that the native oxide layer had been completely removed. After etching for up to 20 min, the Ti felt displayed a smooth surface, which remained unchanged as the etching duration increased (**Supplementary Figure 2**). When the etching time increased above 30 min, the roughness of the Ti felt began to rise (**Supplementary Figure 3**). **Figure 2F** shows the electrochemical double-layer capacitance (C_{dl}) value of the Ti felt with respect to the etching time. Generally, C_{dl} is proportional to the electrochemical surface area (ECSA), and is related to the roughness factors of the surface (Gira et al., 2016). As etching time increased, the C_{dl} value increased from 0.206 mF (0 min) to 1.675 mF (40 min). This indicates that there was an increase in the surface roughness in addition to the surface area of the Ti felt with the etching time

(**Supplementary Figure 4**). The surface morphologies of the IrO_2/Ti electrodes following electrodeposition are shown in **Figure 3** and **Supplementary Figure 5**. The surface roughness of the Ti felt had an effect on the surface roughness of the electrodeposited IrO_2 layer. The IrO_2/Ti-0 electrode (**Figures 3A,B**) displayed cracks on the IrO_2 layer that may be attributed to a high level of internal stress (Suvorov et al., 2018). Conversely, regarding the IrO_2/Ti-30 electrode (**Figures 3C,D**), the coated IrO_2 layer was flat and had minute visible cracks. This observation demonstrates the effect of chemical etching, and also indicates that an increase in etching time results in the removal of surface micro-cracks (Xiao et al., 2017). When the etching time was ≥ 40 min, the formation of IrO_2 agglomerates around the surface roughness as a result of over-etching was observed (**Figures 3E,F**).

The results of the analysis of the structure of the IrO_2/Ti-30 electrode using XRD and X-ray photoelectron spectroscopy (XPS) are shown in **Figure 4**. Its XRD pattern showed no other peaks apart from those corresponding to Ti (**Figure 4A**). **Figure 4B** presented the full scan XPS spectra of IrO_2/Ti-30

FIGURE 5 | (A) Polarization curves of the IrO_2/Ti-0, 10, 20, 30, 40 electrodes using 0.1 M $HClO_4$ electrolyte without iR correction. **(B)** Bar graph showing the overpotential (η) of the geometric activity (20 mA cm^{-2}) and mass activity (20 A g$_{Ir}^{-1}$). **(C)** Comparison of the OER overpotential (10 mA cm^{-2}) obtained in this study with those of other noble metal electro catalyst in acidic condition with iR correction. **(D)** Tafel plots the electrodes with iR correction. **(E)** Variation of electrochemical double layer capacitance (C$_{dl}$) with etching times (0–40 min). **(F)** Chronopotentiometry curves of the IrO_2/Ti-30 (red) and IrO_2/Ti-0 (blue) electrodes under a constant current density of 10 mA cm^{-2}.

electrode. Additionally, its Ir 4f XPS spectra showed peaks at 65.1 eV ($4f_{5/2}$) and 62.1 eV ($4f_{7/2}$), which corresponded to the Ir^{3+} state, and others at 66.4 eV ($4f_{5/2}$) and 63.5 eV ($4f_{7/2}$), which corresponded to the unscreened component of the Ir^{4+} state (**Figure 4C**) (Choe et al., 2018). In the O 1s region of the high-resolution spectra of the IrO_2/Ti-30 electrode, peaks corresponding to OH and O were observed at 530.9 and 529.6 eV, respectively (**Figure 4D**). Additionally, amorphous IrO_2 demonstrated a higher hydroxide concentration than crystalline IrO_2, indicating that the IrO_2 layer on the Ti felt consisted of amorphous IrO_2 (Jiang et al., 2019).

To evaluate the variation of the OER catalytic activity of the IrO_2/Ti electrodes with etching time, electrochemical analyses were performed using 0.1 M $HClO_4$ as the electrolyte, and the results obtained are illustrated in **Figure 5**. At 20 mA cm^{-2}, the overpotential values corresponding to IrO_2/Ti-0, IrO_2/Ti-10, IrO_2/Ti-20, IrO_2/Ti-30, and IrO_2/Ti-40, were 462, 401, 382, 370, and 419 mV, respectively (**Figure 5A**). Thus, the IrO_2/Ti-30 electrode showed the highest OER activity. To determine the effect of etching time on the Ir loading mass, ICP-MS was performed. Observations revealed that as the etching time increased, the Ir loading mass increased from 0.183 mg cm^{-2} (IrO_2/Ti-0) to 0.234 mg cm^{-2} (IrO_2/Ti-20) (**Supplementary Figure 6**). After 30 min of etching, the loading mass began to decrease, dropping to 0.198 mg cm^{-2} (IrO_2/Ti-40) at 40 min. Based on these Ir loading masses, the overpotential was recorded at 20 A g$_{Ir}^{-1}$ of mass activity (**Figure 5B**). The IrO_2/Ti-30

electrode also showed the lowest overpotential value at 240 mV, and a comparison of the Ir mass activity at 2.0 V (vs. RHE), revealed the best OER performance (**Supplementary Figure 7**). When the IrO_2 loading was excessive, some of the internal surfaces of the IrO_2 layer could not be fully utilized (Zhang et al., 2020); thus, the IrO_2/Ti-30 electrode showed superior catalytic performance relative to the IrO_2/Ti-20 electrode, which had the largest IrO_2 loading mass. The overpotentials shown in the iR-corrected LSV curve of the IrO_2/Ti-30 electrode were compared with other noble metal electrocatalysts under acidic pH conditions (**Supplementary Figure 8**). The results obtained demonstrated that the IrO_2/Ti-30 electrode had the lowest overpotential (**Figure 5C** and **Supplementary Table 1**). The Tafel slope derived from the iR-corrected LSV curve, which was calculated according to Equation (1), is shown in **Figure 5D**.

$$\eta = A \times log\left(\frac{i}{i_0}\right) \tag{1}$$

where η, i, i$_0$, and A represent the overpotential, current density, exchange current density, and the Tafel slope, respectively (Fang and Liu, 2014). The Tafel slope of the IrO_2/Ti-30 electrode was 51 mV dec^{-1}, which is lower than those of IrO_2/Ti-0 (119 mV dec^{-1}), IrO_2/Ti-10 (67 mV dec^{-1}), IrO_2/Ti-20 (54 mV dec^{-1}), and IrO_2/Ti-40 (88 mV dec^{-1}), indicating that the IrO_2/Ti-30 electrode surface results in faster reaction rates in the OER. Hence, this demonstrates superior catalytic activity. ECSA

enhancement implies an increase in the number of accessible Ir active sites (Zhang et al., 2020). Therefore, electrodes with large ECSA tend to exhibit superior catalytic activity. The capacitance value (C_{dl}) of the IrO_2/Ti-30 electrode, which is proportional to ECSA, was 0.755 mF. This C_{dl} value was higher than those of IrO_2/Ti-0, IrO_2/Ti-10, IrO_2/Ti-20, and IrO_2/Ti-40, which were 0.267, 0.569, 0.580, and 0.639 mF, respectively (**Figure 5E** and **Supplementary Figure 9**). Thus, it was reasonable to consider that the increase in ECSA could be attributed to the increase in surface roughness in the IrO_2/Ti-30 electrode, leading to an enhancement of OER activity. When examining the IrO_2/Ti-40 electrode, there was an increase in surface roughness, however, the formation of agglomerates on the surface, as shown in its SEM image, resulted in a decrease in specific surface area. This in turn resulted in a decrease in catalytic activity with respect to the OER (Hara et al., 2018).

The enhanced OER activity of the amorphous IrO_2/Ti-30 electrode was attributed to its high surface area (Bernicke et al., 2015). The superior OER activity of the IrO_2/Ti-30 electrode could also be attributed to the large amount of iridium hydroxide its surface. Under acidic conditions, the hydroxide of the amorphous IrO_2 surface can react to form electrophilic O^{I-} species ($Ir^xO^{II-}H \rightleftharpoons Ir^xO^{I-} + H^+ + e^-$). These species are susceptible to attack by water molecules or OH species; thus, the potential-determining step and rate-limiting step of the OER, resulting in the formation of O-O bonds, can be accelerated (Jiang et al., 2019). Therefore, the presence of hydroxide species on the surface of the IrO_2 layer lower the adsorption energy required to attract H_2O molecules. This leads to the accumulation of oxidation equivalents, which are associated with enhanced OER activity, at reaction sites (Bergmann et al., 2015). The study of the stability of the IrO_2 catalyst layers revealed that the IrO_2/Ti-30 electrode showed the highest OER activity and was evaluated using 0.1 M $HClO_4$ as electrolyte at 25°C. The variation of its potential with time owing to the application of a constant current density of 10 mA cm^{-2} is shown in **Figure 5F**. After ~800 min, it was observed that its stability was higher than that of the IrO_2/Ti-0 electrode. This superior stability could be attributed to the IrO_2 catalyst layer, which serves as a passivation layer that protected the Ti felt from corrosion.

CONCLUSION

In this study, an electrode for the OER was prepared via the electrodeposition of an amorphous IrO_2-based catalyst on Ti felt. To increase the surface area of the Ti felt before the electrodeposition, its surface roughness was increased *via* wet etching. Thus, after etching for 30 min, there was an increase in its surface roughness, and the amorphous IrO_2 layer was uniformly deposited. This resulted in superior OER catalytic activity in comparison with the deposition of the crystalline phase, owing to the presence of surface iridium hydroxide. Additionally, the IrO_2/Ti-30 electrode showed superior OER catalytic activity and mass activity, which may be attributed to an increase in active sites owing to an increase in surface roughness. Stability tests that lasted ~800 min also confirmed its excellent stability in comparison with the IrO_2/Ti-0 electrode. This electrode with increased surface roughness and excellent stability, prepared via electrodeposition and etching, demonstrated superior OER catalytic performance under acidic conditions. Therefore, the results of this study can serve as a promising path for the production of high-performance and low-cost OER electrodes for application in proton exchange membrane water electrolysis.

DATA AVAILABILITY STATEMENT

All datasets generated for this study are included in the article/**Supplementary Material**.

AUTHOR CONTRIBUTIONS

YJP and JL conceived the idea and designed the experiments. YJP, YSP, and SC synthesized the electrocatalysts and evaluated their electrochemical properties. JY and MJ performed the structure analysis. JL and JJ performed the physical characterizations. JWL, J-DK, and SMC coordinated and supervised the overall project. All authors reviewed the final manuscript.

FUNDING

SUPPLEMENTARY MATERIAL

The Supplementary Material for this article can be found online at: https://www.frontiersin.org/articles/10.3389/fchem.2020.593272/full#supplementary-material

REFERENCES

Al-Shroofy, M., Zhang, Q., Xu, J., Chen, T., Kaur, A. P., and Cheng, Y.-T. (2017). Solvent-free dry powder coating process for low-cost manufacturing of LiNi$_{1/3}$ Mn$_{1/3}$Co$_{1/3}$O$_2$ cathodes in lithium-ion batteries. *J. Power Sources* 352, 187–193. doi: 10.1016/j.jpowsour.2017.03.131

Bensaid, S., Centi, G., Garrone, E., Perathoner, S., and Saracco, G. (2012). Towards artificial leaves for solar hydrogen and fuels from carbon dioxide. *ChemSusChem* 5, 500–521. doi: 10.1002/cssc.201100661

Bergmann, A., Martinez-Moreno, E., Teschner, D., Chernev, P., Gliech, M., de Araújo, J. F., et al. (2015). Reversible amorphization and the catalytically active state of crystalline Co$_3$O$_4$ during oxygen evolution. *Nat. Commun.* 6:8625. doi: 10.1038/ncomms9625

Bernicke, M., Ortel, E., Reier, T., Bergmann, A., Ferreira de Araujo, J. F., Strasser, P., et al. (2015). Iridium oxide coatings with templated porosity as highly active oxygen evolution catalysts: Structure-activity relationships. *ChemSusChem* 8, 1908–1915. doi: 10.1002/cssc.2014 02988

Brillet, J., Yum, J.-H., Cornuz, M., Hisatomi, T., Solarska, R., Augustynski, J., et al. (2012). Highly efficient water splitting by a dual-absorber tandem cell. *Nat. Photon.* 6, 824–828. doi: 10.1038/nphoton.2012.265

Bryce, G., Severi, S., Van Hoof, R., Guo, B., Kunnen, E., Witvrouw, A., et al. (2010). Development, optimization and evaluation of a CF_4 pretreatment process to remove unwanted interfacial layers in stacks of CVD and PECVD polycrystalline silicon-germanium for MEMS applications. *ECS Transactions* 28:9. doi: 10.1149/1.3489934

Chalker, P. R., Bull, S. J., and Rickerby, D. S. (1991). A review of the methods for the evaluation of coating-substrate adhesion. *Mater. Sci. Eng. A* 140, 583–592. doi: 10.1016/0921-5093(91)90482-3

Choe, S., Lee, B.-S., Cho, M. K., Kim, H.-J., Henkensmeier, D., Yoo, S. J., et al. (2018). Electrodeposited IrO_2/Ti electrodes as durable and cost-effective anodes in high-temperature polymer-membrane-electrolyte water electrolyzers. *Appl. Cat. B* 226, 289–294. doi: 10.1016/j.apcatb.2017.12.037

Choi, W., Jang, M. J., Park, Y. S., Lee, K.-H., Lee, J. Y., Seo, M. H., et al. (2018). Three-dimensional honeycomb-like $Cu_{0.81}Co_{2.19}O_4$ nanosheet arrays supported by nickel foam and their high efficiency as oxygen evolution electrode. *ACS Appl. Mater. Interfaces.* 10, 38663–38668. doi: 10.1021/acsami.8b12478

Dincă, M., Surendranath, Y., and Nocera, D. G. (2010). Nickel-borate oxygen-evolving catalyst that functions under benign conditions. *Proc. Natl. Acad. Sci U. S. A.* 107, 10337–41. doi: 10.1073/pnas.1001859107

Fan, L., Zhuang, H. L., Zhang, W., Fu, Y., Liao, Z., and Lu, Y. (2018). Stable lithium electrodeposition at ultra-high current densities enabled by 3D PMF/Li composite anode. *Adv. Energy Mater.* 8:1703360. doi: 10.1002/aenm.201 703360

Fang, Y.-H., and Liu, Z.-P. (2014). Tafel kinetics of electrocatalytic reactions: from experiment to first-principles. *ACS Catal.* 4, 4364–4376. doi: 10.1021/cs501312v

Fouda-Onana, F., Guillet, N., and AlMayouf, A. M. (2014). Modified pulse electrodeposition of Pt nanocatalyst as high-performance electrode for PEMFC. *J. Power Sources* 271, 401–405. doi: 10.1016/j.jpowsour.2014.08.031

Gira, M. J., Tkacz, K. P., and Hampton, J. R. (2016). Physical and electrochemical area determination of electrodeposited Ni, Co, and NiCo thin films. *Nano Converg.* 3:6. doi: 10.1186/s40580-016-0063-0

Guo, Q., Li, X., Wei, H., Liu, Y., Li, L., Yang, X., et al. (2019). Sr, Fe co-doped perovskite oxides with high performance for oxygen evolution reaction. *Front. Chem.* 7:224. doi: 10.3389/fchem.2019.00224

Hara, M., Badam, R., Wang, G. J., Huang, H. H., and Yoshimura, M. (2018). Synthesis and evaluation of iridium oxide nanoparticle catalysts supported on nitrogen-doped reduced graphene oxides. *ECS Trans.* 85, 27–35. doi: 10.1149/08511.0027ecst

Jang, M. J., Yang, J., Lee, J., Park, Y. S., Jeong, J., Park, S. M., et al. (2020). Superior performance and stability of anion exchange membrane water electrolysis: pH-controlled copper cobalt oxide nanoparticles for the oxygen evolution reaction. *J. Mater. Chem. A* 8, 4290–4299. doi: 10.1039/C9TA1 3137J

Jiang, B., Kim, J., Guo, Y., Wu, K. C. W., Alshehri, S. M., Ahamad, T., et al. (2019). Efficient oxygen evolution on mesoporous IrO_x nanosheets. *Catal. Sci. Technol.* 9, 3697–3702. doi: 10.1039/C9CY0 0302A

Kanan, M. W., and Nocera, D. G. (2008). *In situ* formation of an oxygen-evolving catalyst in neutral water containing phosphate and Co^{2+}. *Science* 321, 1072–1075. doi: 10.1126/science.1162018

Kim, H., Subramanian, N. P., and Popov, B. N. (2004). Preparation of PEM fuel cell electrodes using pulse electrodeposition. *J. Power Sources* 138, 14–24. doi: 10.1016/j.jpowsour.2004.06.012

Lee, B., Ahn, S. H., Park, H., Choi, I., Yoo, S. J., Kim, H., et al. (2015). Development of electrodeposited IrO_2 electrodes as anodes in polymer electrolyte membrane water electrolysis. *Appl. Cat. B* 179, 285–291. doi: 10.1016/j.apcatb.2015. 05.027

Lee, B.-S., Park, H.-Y., Choi, I., Cho, M. K., Kim, H.-J., Yoo, S. J., et al. (2016). Polarization characteristics of a low catalyst loading PEM water electrolyzer operating at elevated temperature. *J. Power Sources* 309, 127–134. doi: 10.1016/j.jpowsour.2015.12.139

Maliar, T., Cesiulis, H., and Podlaha, E. J. (2019). Coupled electrodeposition of Fe–Co–W alloys: thin films and nanowires. *Front. Chem.* 7:542. doi: 10.3389/fchem.2019.00542

Marzouk, S. A. M. (2003). Improved electrodeposited iridium oxide pH sensor fabricated on etched titanium substrates. *Anal. Chem.* 75, 1258–1266. doi: 10.1021/ac0261404

Nam, J. H., Jang, M. J., Jang, H. Y., Park, W., Wang, X., Choi, S. M., et al. (2019). Room-temperature sputtered electrocatalyst WSe_2 nanomaterials for hydrogen evolution reaction. *J. Energy Chem.* 57, 107–111 doi: 10.1016/j.jechem.2019.11.027

Park, Y. S., Choi, W.-S., Jang, M. J., Lee, J. H., Park, S., Choi, S. M., et al. (2019a). Three-dimensional dendritic Cu–Co–P electrode by one-step electrodeposition on a hydrogen bubble template for hydrogen evolution reaction. *ACS Sustain Chem. Eng.* 7, 10734–10741. doi: 10.1021/acssuschemeng. 9b01426

Park, Y. S., Jang, M. J., Jeong, J., Park, S. M., Wang, X., Seo, M. H., et al. (2020a). Hierarchical chestnut-burr like structure of copper cobalt oxide electrocatalyst directly grown on Ni foam for anion exchange membrane water electrolysis. *ACS Sustain. Chem. Eng.* 8, 2344–2349. doi: 10.1021/acssuschemeng. 9b06767

Park, Y. S., Lee, J. H., Jang, M. J., Jeong, J., Park, S. M., Choi, W.-S., et al. (2019b). Co3S4 nanosheets on Ni foam via electrodeposition with sulfurization as highly active electrocatalysts for anion exchange membrane electrolyzer. *Int. J. Hydrogen Energ.* 45, 36–45. doi: 10.1016/j.ijhydene.2019. 10.169

Park, Y. S., Yang, J., Lee, J., Jang, M. J., Jeong, J., Choi, W.-S., et al. (2020b). Superior performance of anion exchange membrane water electrolyzer: ensemble of producing oxygen vacancies and controlling mass transfer resistance. *Appl. Catal. B Environ.* 278:119276. doi: 10.1016/j.apcatb.2020.119276

Sapountzi, F. M., Divane, S. C., Papaioannou, E. I., Souentie, S., and Vayenas, C. G. (2011). The role of nafion content in sputtered IrO_2 based anodes for low temperature PEM water electrolysis. *J. Electroanal Chem.* 662, 116–122. doi: 10.1016/j.jelechem.2011.04.005

Smith, R. D. L., Sporinova, B., Fagan, R. D., Trudel, S., and Berlinguette, C. P. (2014). Facile photochemical preparation of amorphous iridium oxide films for water oxidation catalysis. *Chem. Mater.* 26, 1654–1659. doi: 10.1021/cm4041715

Su, H., Bladergroen, B. J., Linkov, V., Pasupathi, S., and Ji, S. (2011). Study of catalyst sprayed membrane under irradiation method to prepare high performance membrane electrode assemblies for solid polymer electrolyte water electrolysis. *Int. J. Hydrogen Energ.* 36, 15081–15088. doi: 10.1016/j.ijhydene.2011.08.057

Suen, N. T., Hung, S. F., Quan, Q., Zhang, N., Xu, Y. J., and Chen, H. M. (2017). Electrocatalysis for the oxygen evolution reaction: recent development and future perspectives. *Chem. Soc. Rev.* 46, 337–365. doi: 10.1039/C6CS00328A

Suvorov, D., Gololobov, G., Tarabrin, D., Slivkin, E., Karabanov, S., and Tolstoguzov, A. (2018). Electrochemical deposition of Ni–W crack-free coatings. *Coatings* 8:233. doi: 10.3390/coatings8070233

Wang, G., Li, J., Lv, K., Zhang, W., Ding, X., Yang, G., et al. (2016). Surface thermal oxidation on titanium implants to enhance osteogenic activity and *in vivo* osseointegration. *Sci. Rep.* 6:31769. doi: 10.1038/srep31769

Wang, N., Sun, B., Zhao, P., Yao, M., Hu, W., and Komarneni, S. (2018). Electrodeposition preparation of NiCo 2 O 4 mesoporous film on ultrafine nickel wire for flexible asymmetric supercapacitors. *Chem. Eng. J.* 345, 31–38. doi: 10.1016/j.cej.2018.03.147

Xiao, H., Wang, H., Fu, G., and Chen, Z. (2017). Surface roughness and morphology evolution of optical glass with micro-cracks during chemical etching. *Appl. Opt.* 56, 702–711. doi: 10.1364/AO.56.000702

Xiaokai, A., Yang, C., Wu, Z., Liu, L., Li, S., Zhou, L., et al. (2019). Self-regulated super-hydrophobic Cu/CuO electrode film deposited by one-step high-power sputtering. *Adv. Electron. Mater.* 6:1900891. doi: 10.1002/aelm.201900891

Yagi, M., Tomita, E., and Kuwabara, T. (2005). Remarkably high activity of electrodeposited IrO_2 film for electrocatalytic water oxidation. *J. Electroanal. Chem.* 579, 83–88. doi: 10.1016/j.jelechem.2005. 01.030

Zhang, K., Mai, W., Li, J., Wang, H., Li, G., and Hu, W. (2020). Highly scattered ir oxides on TiN as an efficient oxygen evolution reaction electrocatalyst in acidic media. *J. Mater. Sci.* 55, 3507–3520. doi: 10.1007/s10853-019-04 201-4

Zhou, X., Qi, W., Yin, K., Zhang, N., Gong, S., Li, Z., et al. (2020). $Co(OH)_2$ nanosheets supported on laser ablated cu foam: an efficient oxygen evolution reaction electrocatalyst. *Front. Chem.* 7:900. doi: 10.3389/fchem.2019.00900